Hindawi
Shock and Vibration
Volume 2019, Article ID 8240586, 10 pages
https://doi.org/10.1155/2019/8240586

Research Article

Transmission of Normal P-Waves across a Single Joint Based on g-λ Model

Zhanfeng Fan,[1] Jichun Zhang,[1] Hua Xu ,[1] and Jianhua Cai[2]

[1]*School of Civil Engineering, Southwest Jiaotong University, Chengdu 610031, China*
[2]*China Railway Southwest Research Institute Co. LTD, Chengdu 611731, China*

Correspondence should be addressed to Hua Xu; xuhua@home.swjtu.edu.cn

Received 14 February 2019; Accepted 10 April 2019; Published 11 June 2019

Academic Editor: Jean-Mathieu Mencik

This paper investigates the wave transmission and reflection of an elastic P-wave at a single joint for normal incidence. First, considering a coupled joint (correction parameter λ, $0 < \lambda < 1$), a normal deformation constitutive model of the joint (g-λ model) under static or quasi-static loading is introduced and then extended to dynamic loading. The nonlinearity of the joint stress-deformation curve increases with increasing λ. Second, the interaction between the P-wave and the joint is investigated by using the method of characteristics and the displacement discontinuity method to deduce the differential expression of the transmitted wave's particle velocity. The approximate analytical expressions of the transmission and reflection coefficients are obtained according to the Lemaitre equivalent strain assumption. Third, parametric studies are conducted to evaluate the effects of λ on transmission characteristics for a normally incident P-wave at a single joint. The results show that the particle velocity of the transmitted wave depends on λ. When λ takes the limit values 0 and 1, the transmitted wave's particle velocities are then consistent with the conclusions of the classical exponential model and the Barton–Bandis model. In addition, the transmission and reflection coefficients are discussed with respect to λ and also to the ratio of the joint closure to the maximum allowable joint closure.

1. Introduction

In Earth's crust, discontinuities, such as faults, joints, bedding planes, and fractures, are ubiquitous and they often control the hydraulic and mechanical behavior of rock masses [1–4]. Elastic waves propagating through jointed rock masses will attenuate (or slow down) because of the existence of abundant rock joints [5–9]. The properties of the jointed rock mass including the joint matching coefficient (JMC), joint roughness coefficient (JRC), and the joint stiffness affect not only the dynamic behavior of joint but also the stress wave energy attenuation confirmed by the laboratory experiment (i.e., split Hopkinson pressure bar (SHPB) and ultrasonic test) [10–12]. Other factors, such as rock acoustic impedance and rock thermal effect, also affect the stress wave propagation across the jointed rock mass [13, 14]. Due to these facts, it is necessary to further study the interaction between the P-wave and the joint to prove serving the application of the elastic waves in rock engineering.

Different constitutive models have been presented to investigate the deformation characteristics of a jointed rock mass under static or quasi-static loading/unloading. Amongst them, the Barton–Bandis (BB) model, a modification of Goodman's hyperbolic model [15, 16], is widely used to describe the nonlinear deformation behavior of a single joint [17, 18]. Although the BB model is established under the quasi-static or cyclic loading condition, it is reasonable for the dynamic condition because jointed rock masses have experienced multiple deformations in geological history [19]. Many researchers have investigated the P-wave propagating through the joint based on the BB model [5, 20–22]. However, since the BB model is based on experimental data of five kinds of jointed rock masses (slate, dolerite, limestone, siltstone, and sandstone), it may not be universally applicable to all other jointed rock masses. Some improved constitutive models for jointed rock masses are proposed or deduced from different experimental data or mathematical principles. For instance, the matrix of

compliance components for a rock joint was adopted to describe the stress-deformation relations under compression and shear loads [23]. The relationship between constant normal stress and time-dependent closure was formulated as a function of time in terms of the aperture distribution of a fracture and the relaxation modulus of rock [24]. With introducing a half-closed stress and correction parameters, Malama and Kulatilake [25] presented a generalized semi-empirical exponential model, which can better fit the results of fracture closure experiments of jointed diorite and granodiorite rock specimens under monotonically increasing normal compressive loading. Yu et al. [26] proposed a 3-parameter constitutive model, which overcame the mathematical defects of the BB model and the classical exponential model. Following Yu's viewpoint, Rong et al. [27] established the g-δ model ($0 < \delta < 1$) and the g-λ model ($0 < \lambda < +\infty$) under static or quasi-static loading. The results indicated that the g-λ model can be more suitable for the coupled ($0 < \lambda < 1$) and uncoupled ($\lambda \geq 1$) joint. However, the g-λ model has been made up for the mathematical defects and been verified by different experimental data. The collection parameter λ can be adjusted at the medium stress level, and the stress-deformation curve of the joint was more applicable than the classical exponential model and the BB model. The classical exponential model and the BB model have been extended to dynamic loading [19, 20]. The g-λ model's dynamic characteristic is yet neglected.

In this paper, considering a coupled joint ($0 < \lambda < 1$), a normal deformation constitutive model of the joint (g-λ model) under static or quasi-static loading is introduced first and then extended to dynamic loading. Second, the finite difference formula suitable for transmitted wave's particle velocity is obtained found on the method of characteristics (MC) [5, 19, 22, 28] and the displacement discontinuity method (DDM) [29–33]. The approximate analytic solutions of the transmission and reflection coefficients are deduced theoretically based on damage mechanics. Finally, parametric studies and discussions of a P-wave transmission across a single joint which is regarded as a nonwelded interface are conducted according to the MATLAB numerical program. The results show that the parameter λ has a significant effect on the dynamic characteristics of the reflected and transmitted waves.

2. Theoretical Formulations

2.1. Dynamic Expansion of the g-λ Model. The g-λ model is a normal deformation constitutive model of a single joint and can be applied to both the coupled and uncoupled joint [27]. One of the key features of the g-λ model is adding the correction parameter λ (dimensionless) to speed up the normal deformation. The g-λ model is formulated as follows:

$$d_n = d_{ma}\left[1 - \left(\frac{\lambda\sigma_n}{d_{ma}k_{ni}} + 1\right)^{-(1/\lambda)}\right], \tag{1}$$

where d_n and d_{ma} denote the joint closure and the maximum allowable closure of the joint, respectively, k_{ni} is the joint normal stiffness at initial stress, and σ_n is the normal effective stress. The values of d_{ma} and k_{ni} can be determined from the laboratory measurements on JRC, joint surface compressive strength (JCS), and average aperture thickness (a_j) [17, 18]. The parameter λ is in association with joint weathering, roughness, fluctuation degree, matching of the joint surface, and strength of the wall of rock joints. In this paper, we only consider the case of $0 < \lambda < 1$ for the coupled joint. The joint is assumed to be planar, large in extent, and small in thickness compared to the wavelength, and the joint and the intact rock are linearly elastic. If $\lambda \longrightarrow 0$, according to the L'Hospital's rule, the exponential term in equation (1) can be obtained as follows:

$$\begin{aligned}\lim_{\lambda\longrightarrow 0}\left(\frac{\lambda\sigma_n}{k_{ni}d_{ma}} + 1\right)^{-(1/\lambda)} &= \exp\left\{\lim_{\lambda\longrightarrow 0}\left[-\frac{1}{\lambda}\ln\left(\frac{\lambda\sigma_n}{k_{ni}d_{ma}} + 1\right)\right]\right\} \\ &= \exp\left(-\frac{\sigma_n}{k_{ni}d_{ma}}\right),\end{aligned} \tag{2}$$

to give

$$d_n\big|_{\lambda\longrightarrow 0} = d_{ma}\left[1 - \exp\left(-\frac{\sigma_n}{k_{ni}d_{ma}}\right)\right]. \tag{3}$$

That is, the classical exponential model is recovered for $\lambda \longrightarrow 0$. On the contrary, when $\lambda \longrightarrow 1$, the exponential term in equation (1) becomes

$$\lim_{\lambda\longrightarrow 1}\left(\frac{\lambda\sigma_n}{k_{ni}d_{ma}} + 1\right)^{-(1/\lambda)} = \frac{k_{ni}d_{ma}}{\sigma_n + k_{ni}d_{ma}}. \tag{4}$$

Substituting equation (4) in (1), we get

$$d_n\big|_{\lambda\longrightarrow 1} = \frac{\sigma_n}{k_{ni} + (\sigma_n/d_{ma})}, \tag{5}$$

and thus, the BB model is a special case of the g-λ model.

The schematic curves of the g-λ model with different values of λ, the BB model, and the classical exponential model of normal deformational behavior of a single joint are shown in Figure 1. The tangent slope of each curve can be defined as the joint stiffness ($k_n = (\Delta\sigma_n/\Delta d_n)$) [19]. Compared to the linear model, the g-λ model, the BB model, and the classical exponential model involve the joint stiffness that increases with the increasing normal effective stress. When the normal stress increases nearly to an infinite value ($\sigma_n \longrightarrow \infty$), the joint closure of each model approaches the maximum allowable closure ($d_n \longrightarrow d_{ma}$). The curve of the g-λ model is between the BB model and the classical exponential model. In addition, the tangent slope of the g-λ model's curve increases with the increase of λ, which means that the degree of nonlinearity increases.

In the meantime, the g-λ model has been validated to be more suitable than other models by fitting different experimental results. The normal deformation of the BB model is less than test data, and the normal deformation of the classical exponential model is greater than it under the intermediate stress level, as shown in Figure 2. Under the high stress level, the approach speed of normal deformation

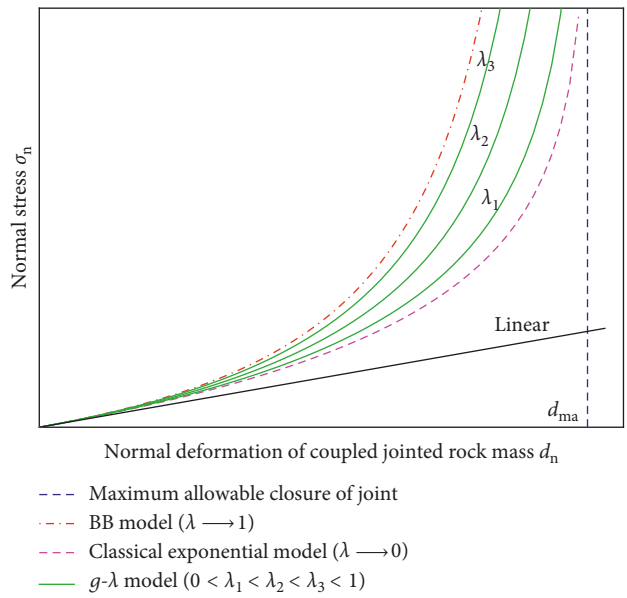

Figure 1: Scheme of the g-λ model with different values of λ, the BB model, and the classical exponential model of normal deformational behavior of a single joint (where $\lambda = \lambda_i$, in which $i = 1, 2, 3$).

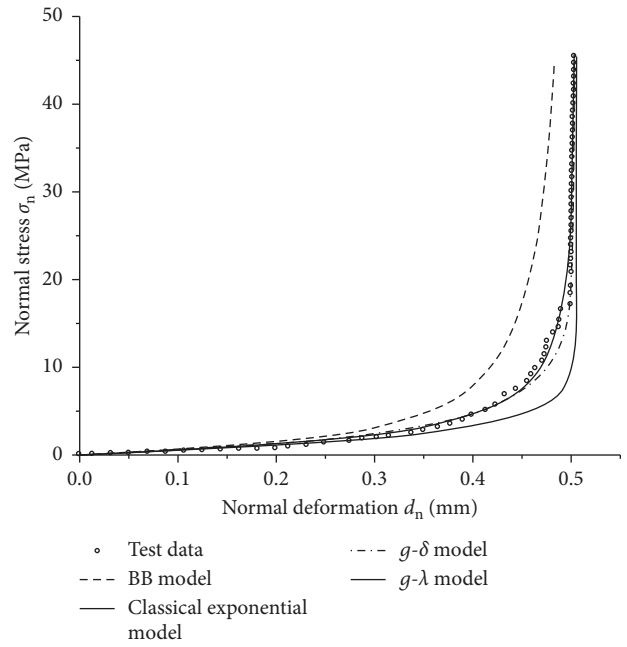

Figure 2: Experiment of a single joint in Arizona granodiorite [25] under compression and simulation [27].

in the BB model to the maximum joint closure is lower than that of the test data. The g-δ model and the g-λ model are more consistent with experimental data. Of them, the g-λ model fits best, where $\lambda = 0.41$ [27].

A large body of literature has confirmed that continuous cyclic loading and unloading can make the stress-deformation relationship become the elastic relationship without a hysteresis loop because natural rock joints undergo many deformations in the long geological history [5, 19, 20, 34]. Therefore, the hysteresis phenomenon in the initial cyclic loading and unloading process and the influence of the loading rate on the joint deformation can be neglected. It is reasonable for the application of the BB model and the classical exponential model in the wave propagation. This viewpoint is borrowed in the present study to extend the g-λ model to the dynamic condition for computational analysis.

2.2. Method of Characteristics. It is assumed that a joint exists at $x = x_1$ in a half-space of a linear elastic, homogeneous and isotropic medium. When a normal incidence plane P-wave impinges upon the boundary of the half-space, a reflected wave and a transmitted wave will be generated at the joint. Through the linear elastic DDM which has been applied to wave propagation, the stresses on the two sides of the joint are assumed to be continuous while the difference in displacements equals the closure (opening) of joint, which can be, respectively, expressed as follows:

$$\sigma(x_1, t) = \sigma(x_1 + d_n, t), \tag{6}$$

where $\sigma(x_1, t)$ and $\sigma(x_1 + d_n, t)$ are the normal stress before and after the P-wave through the joint, respectively. Based on equation (1), the displacement difference between the two sides of the joint is

$$u(x_1, t) - u(x_1 + d_n, t) = d_{ma}\left[1 - \left(\frac{\lambda\sigma(x_1, t)}{d_{ma}k_{ni}} + 1\right)^{-(1/\lambda)}\right], \tag{7}$$

where $u(x_1, t)$ and $u(x_1 + d_n, t)$ are the displacement before and after the P-wave across the joint, respectively.

The derivative expression of equation (7) is as follows:

$$\frac{\partial u(x_1, t)}{\partial t} - \frac{\partial u(x_1 + d_n, t)}{\partial t} = v(x_1, t) - v(x_1 + d_n, t) = \frac{\left(\left(\left(\lambda\sigma(x_1, t)\right)/\left(d_{ma}k_{ni}\right)\right) + 1\right)^{-((\lambda+1)/\lambda)}}{k_{ni}} \frac{\partial\sigma(x_1, t)}{\partial t}, \tag{8}$$

where $v(x_1, t)$ and $v(x_1 + d_n, t)$ are the particle velocity before and after the P-wave through the joint, respectively.

The method of characteristics has been widely used for solving the problems of one-dimensional wave propagation in continuous linearly elastic media, as shown in Figure 3. The relations of the particle velocity v and the stress σ can be derived as

$$\begin{cases} zv(x_1, t) - \sigma(x_1, t) = \text{const}, \\ \quad \text{left} - \text{running characteristic line}, \\ zv(x_1, t) + \sigma(x_1, t) = \text{const}, \\ \quad \text{right} - \text{running characteristic line}, \end{cases} \tag{9}$$

where z is the rock acoustic impedance and equal to the product of the rock density ρ and the rock P-wave velocity v_p.

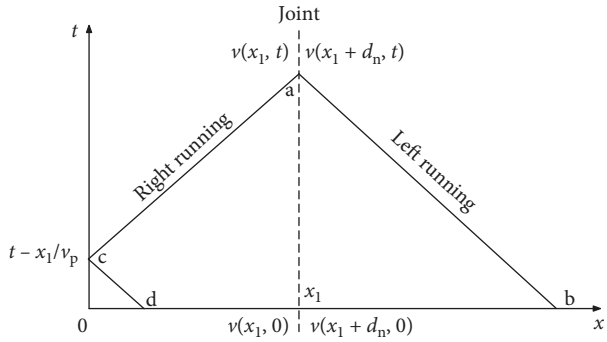

Figure 3: Scheme of left- and right-running characteristics in the x-t plane.

Since the half-space is undisturbed at $t=0$, both the particle velocity $v(x,t)$ and the stress $\sigma(x,t)$ are zero at every point of the x-axis. Therefore, along left-running characteristic line ab,

$$zv(x_1+d_n,t)-\sigma(x_1,t)=0. \tag{10}$$

Similarly, along the right-running characteristic line ac,

$$zv(x_1,t)+\sigma(x_1,t)=zp\left(t-\frac{x_1}{v_p}\right)+\sigma\left(0,t-\frac{x_1}{v_p}\right), \tag{11}$$

where $p(t-(x_1/v_p))$ is the particle velocity input to the boundary at time $t-(x_1/v_p)$ and $\sigma(0,t-(x_1/v_p))$ is the stress for $x_1=0$ at time $t-(x_1/v_p)$.

Along another left-running characteristic line cd,

$$zp\left(t-\frac{x_1}{v_p}\right)-\sigma\left(0,t-\frac{x_1}{v_p}\right)=0. \tag{12}$$

Summing up equations (11) and (12) yields

$$zv(x_1,t)+\sigma(x_1,t)=2zp\left(t-\frac{x_1}{v_p}\right). \tag{13}$$

Based on equations (10) and (13), the relation between the particle velocity before and after the joint can be expressed as follows:

$$v(x_1,t)+v(x_1+d_n,t)=2p\left(t-\frac{x_1}{v_p}\right). \tag{14}$$

Substituting equations (8) and (10) into (14), we can derive $((\partial v(x_1+d_n,t))/\partial t)$ as follows:

$$\frac{\partial v(x_1+d_n,t)}{\partial t}=\frac{2k_{ni}}{z}\left[p\left(t-\frac{x_1}{v_p}\right)-v(x_1+d_n,t)\right]\cdot\left[\frac{\lambda z v(x_1+d_n,t)}{d_{ma}k_{ni}}+1\right]^{(\lambda+1)/\lambda}. \tag{15}$$

Similarly, if $\lambda\longrightarrow 0$, on repeating the above derivation process we can obtain $((\partial v(x_1+d_n,t))/\partial t)$ as follows:

$$\frac{\partial v(x_1+d_n,t)}{\partial t}=\frac{2k_{ni}}{z}\left[p\left(t-\frac{x_1}{v_p}\right)-v(x_1+d_n,t)\right]\cdot\exp\left[\frac{z v(x_1+d_n,t)}{d_{ma}k_{ni}}\right]. \tag{16}$$

When $\lambda\longrightarrow 1$, the expression of $((\partial v(x_1+d_n,t))/\partial t)$ is consistent with Zhao and Cai [19] as follows:

$$\frac{\partial v(x_1+d_n,t)}{\partial t}=\frac{2p\left(t-\left(x_1/v_p\right)\right)-2v(x_1+d_n,t)}{\left\{\left(z/\left(k_{ni}+\left((zv(x_1,t))/d_{ma}\right)\right)\right)-\left(\left(z^2v(x_1+d_n,t)\right)/\left(d_{ma}\left(k_{ni}+\left((zv(x_1,t))/d_{ma}\right)^2\right)\right)\right)\right\}}. \tag{17}$$

For numerical calculation, equation (15) is expressed in differential form as

$$v\left(x_1+d_n,t_{j+1}\right)=v\left(x_1+d_n,t_j\right)+\frac{2k_{ni}}{z}\left[p\left(t-\left(x_1/v_p\right)\right)-v\left(x_1+d_n,t_j\right)\right]\cdot\left[\frac{\lambda z v\left(x_1+d_n,t_j\right)}{d_{ma}k_{ni}}+1\right]^{((\lambda+1)/\lambda)}\Delta t. \tag{18}$$

where Δt is the time interval. Equation (18) is an iterative calculating equation for calculating $v(x_1+d_n,t_j)$. Following the same viewpoint, equations (16) and (17) also have a corresponding differential iterative formula, respectively. The energy of the transmitted wave is examined by the energy transmission coefficient T_e:

$$T_e=\frac{\sum_{j=t^0_{tra}}^{j=t^0_{tra}+T_{tra}}z\left(v_{tra}\left(x_1,t_j\right)\right)^2\Delta t}{\sum_{j=t^0_{inc}}^{j=t^0_{inc}+T_{inc}}z\left(v_{inc}\left(x_1,t_j\right)\right)^2\Delta t}, \tag{19}$$

where T_{tra} and T_{inc} are the period of transmitted and incident waves, respectively; t^0_{tra} and t^0_{inc} are the initial time of transmitted and incident waves, respectively; $v_{tra}(x_1,t_j)$ and $v_{inc}(x_1,t_j)$ are the particle velocity of transmitted and incident waves at time t_j and position x_1, respectively.

2.3. Transmission Coefficient and Reflection Coefficient. According to the analytical solutions obtained by Schoenberg [29] and Pyrak-Nolte et al. [30], the transmission coefficient T_{lin} and the reflection coefficient R_{lin} of a linear deformation joint in identical rock can be calculated as follows (for compressional/shear wave incidence):

$$T_{\text{lin}} = \frac{2(k/z\omega)}{-i + 2(k/z\omega)},$$
$$\left|T_{\text{lin}}\right| = \left[\frac{4(k/z\omega)^2}{4(k/z\omega)^2 + 1}\right]^{1/2}, \tag{20}$$

where ω is the angular frequency. For compressional wave incidence, k denotes the joint normal stiffness and z has the same definition as in equation (9):

$$R_{\text{lin}} = \frac{i}{-i + 2(k/z\omega)},$$
$$\left|R_{\text{lin}}\right| = \left[\frac{1}{4(k/z\omega)^2 + 1}\right]^{1/2}, \tag{21}$$

where ω, k, and z have the same definition as in equation (20).

In the g-λ model, the flexibility of joint C_{n} is

$$C_{\text{n}} = \frac{1}{K_{\text{n}}} = \frac{\partial d_{\text{n}}}{\partial \sigma_{\text{n}}} = \frac{1}{k_{\text{ni}}}\left(1 - \frac{d_{\text{n}}}{d_{\text{ma}}}\right)^{\lambda+1}, \tag{22}$$

where K_{n} is the equivalent stiffness [27].

In order to obtain the transmission and reflection coefficients for the g-λ model, here, we draw on the basic idea of the Lemaitre equivalent strain assumption in damage mechanics [35] and assume $(1 - (d_{\text{n}}/d_{\text{ma}}))^{\lambda+1}$ to represent the nonlinear coefficient of joint stiffness. The joint normal stiffness k in equations (20) and (21) can be replaced by the equivalent stiffness K_{n} in equation (22). Therefore, the approximate analytical solutions of the transmission coefficient $|T_\lambda|$ and the reflection coefficient $|R_\lambda|$ of the g-λ model can be represented as follows:

$$\left|T_\lambda\right| = \frac{1}{\sqrt{\left[\left(z\omega(1-\gamma)^{\lambda+1}\right)/(2k_{\text{ni}})\right]^2 + 1}}, \tag{23}$$

$$\left|R_\lambda\right| = \frac{1}{\sqrt{\left[(2k_{\text{ni}})/\left(z\omega(1-\gamma)^{\lambda+1}\right)\right]^2 + 1}}, \tag{24}$$

where $\gamma = (d_{\text{n}}/d_{\text{ma}})$ is the ratio of the joint closure to the maximum allowable joint closure. It is found that the obtained $|T_\lambda|$ and $|R_\lambda|$ are in agreement with the corresponding results when γ is equal to 0 [29, 30]. Note that although the transmission and reflection coefficients of a harmonic wave are conducted in the frequency domain, the technique of the inverse fast Fourier transform (IFFT) can be used for an incident wave with the arbitrary waveform to the time domain [36–38].

3. Parametric Study and Discussions

To demonstrate that the g-λ model can be used for wave propagation, different parameters are discussed by the MATLAB numerical program. We mainly analyze the wave transmission and reflection of a P-wave travelling through a nonwelded single joint at normal incidence, including (i) the behavior of the transmitted wave, (ii) the amplitude-dependence and frequency-dependence of the energy transmission, and (iii) the relationship between the transmission/reflection coefficient and γ.

3.1. Particle Velocity of the Transmitted Wave. The threshold values of wave amplitude, such as the peak particle velocity (PPV), are essential to regulate the damage criteria of rock structures in earthquake engineering. The dynamic compressive strength of rock masses is generally much greater than the dynamic tensile strength. The selection of a wavelet does not cause damage to the jointed rock mass. In other words, the dynamic stress generated by the P-wave should be less than the dynamic tensile strength of the jointed rock mass. Using the fast Fourier transform (FFT) and IFFT, any arbitrary incident wave can be expressed as the sum of a series of harmonic waves [36, 37]. Without losing generality, the incident wave is assumed to be a positive part of one-cycle sinusoidal wave as follows:

$$v_{\text{inc}}(0,t) = \begin{cases} A_0 \sin(2\pi f t), & \text{for } 0 \le t \le \dfrac{1}{2f}, \\ 0, & \text{otherwise}, \end{cases} \tag{25}$$

where $v_{\text{inc}}(0,t)$ is the particle velocity of the incident wave at time t and position $x_1 = 0$ and A_0 and f denote the amplitude and the frequency of the incident wave, respectively [21, 39]. The change of the particle velocity for the transmitted wave is analyzed when the half-sine incident wave propagates through a single joint with four different cases of λ, including (i) $\lambda \longrightarrow 0$, (ii) $\lambda = 0.4$, (iii) $\lambda = 0.8$, and (iv) $\lambda \longrightarrow 1$. The key parameters of a jointed rock mass are listed in Table 1.

When an incident wave reaches a joint in the half-space, a reflected wave and a transmitted wave are created and propagate in two opposite directions. According to equation (18) and the difference forms of equations (16) and (17), Figure 4 shows the particle velocities of the transmitted wave on the basis of the g-λ model, the BB model, and the classical exponential model ($A_0 = 0.1$ m/s and $f = 50$ Hz). It is observed that the waveform of the transmitted wave is similar to that of the incident wave, but the phase has a delay. These phenomena are also observed in [19, 30]. The maximum particle velocities of the transmitted wave v_{tra} are 0.0874 m/s, 0.0911 m/s, 0.0937 m/s, and 0.0947 m/s, as $\lambda \longrightarrow 0$, $\lambda = 0.4$, $\lambda = 0.8$, and $\lambda \longrightarrow 1.0$, respectively. The amplitude of the transmitted wave's particle velocity increases gradually with the increase of λ. If $\lambda \longrightarrow 0$, the transmitted wave for the g-λ model is closer to the value of the classical exponential model, and if $\lambda \longrightarrow 1$, it is closer to that of the BB model. These two special cases calculated under the dynamic condition are consistent with those of the static condition. It shows that the extension of the g-λ model from the static loading to the dynamic loading is workable. As shown in Figure 4, more waves are transmitted with the increase of λ (the weaker the degree of weathering, the less the roughness and joint closure) during the transmission of a P-wave pulse. In other words, the increase of the parameter λ will increase the joint stiffness, resulting in more incident waves being transmitted. The values of the joint closure d_{n} calculated by

Table 1: Key parameters of a jointed rock mass [19].

Parameter description	Symbol	Value	Unit
Density of rock	ρ	2400	kg/m^3
Wave velocity of rock	v_p	4500	m/s
Initial normal stiffness of joint	k_{ni}	1.25	GPa/m
Maximum allowable closure of joint	d_{ma}	0.61	mm

Table 2: Joint closure d_n corresponding to the amplitude of the transmitted wave based on the g-λ model.

Parameter	g-λ model			
	$\lambda \longrightarrow 0$	$\lambda = 0.4$	$\lambda = 0.8$	$\lambda \longrightarrow 1.0$
v_{tra} (m/s)	0.0874	0.0911	0.0937	0.0947
d_n (mm)	0.43	0.39	0.36	0.35

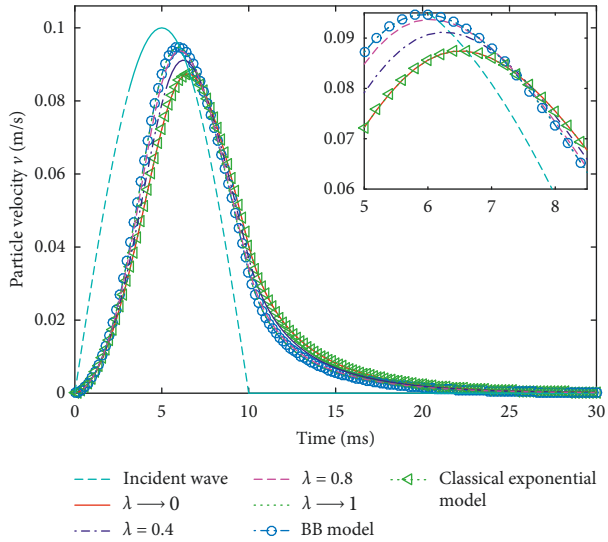

Figure 4: An incident P-wave pulse (v_{int}) and the resulting transmitted pulse (v_{tra}) across a single joint in terms of different constitutive models ($A_0 = 0.1$ m/s and $f = 50$ Hz).

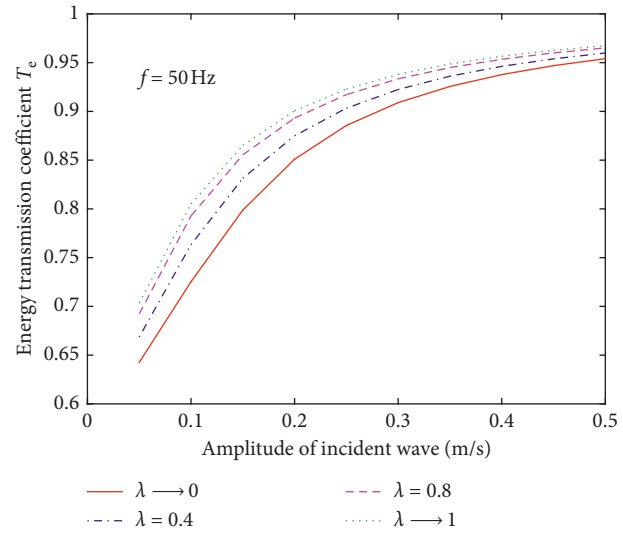

Figure 5: Effect of amplitude on the energy transmission coefficient with different λ values.

equation (23) corresponding to the amplitude of the transmitted wave are listed in Table 2. It can be seen that the joint closure decreases as the parameter λ increases, further indicating that the joint stiffness is gradually increasing.

3.2. Amplitude Dependence and Frequency Dependence of Energy Transmission. In rock engineering, the energy transfer is often concerned when elastic waves propagate through a jointed rock mass. For example, the blast-induced stress waves propagate into the jointed rock mass. Thus, we investigate the properties of amplitude-dependence and frequency-dependence of energy transmission with an incident wave in a form as given in equation (25).

The particle velocity amplitude A_0 is set to a range of 0.05 m/s to 0.5 m/s. The corresponding stress amplitude ($\sigma_{inc} = \rho v_p A_0$) of the incident wave is from 0.54 MPa to 5.4 MPa. The frequency f is still 50 Hz. According to equation (19), the variation of the energy transmission coefficient T_e with respect to the amplitude of the incident wave is shown in Figure 5. If the parameter λ is constant, T_e increases with the increase of the incident wave's amplitude. T_e also increases with the increase of λ when the incident wave's amplitude is fixed. Due to the nonlinear behavior of the joint, the specific stiffness increases with the amplitude of the incident wave which leads to a smaller difference between the joint stiffness and intact rock and more energy transmission.

With different values of λ, the relations of the energy transmission coefficient T_e versus the frequency of the incident wave are shown in Figure 6, where the amplitude A_0 is 0.1 m/s and the frequency f changes from 50 Hz to 1000 Hz. T_e decreases with the increase of the incident wave's frequency. These phenomena indicate that the high-frequency components of the incident wave are filtered out, and only the low-frequency waves pass through. Many literatures have reached this conclusion [19, 21, 30, 32]. The parameter λ has little effect on the energy transmission when the frequency is constant.

3.3. Numerical Calculation of Transmission and Reflection Coefficients. According to equation (23), the transmission coefficient $|T_\lambda|$ for four different values of λ increases until 1 as the parameter γ (the ratio of the joint closure to the maximum allowable joint closure) increases until 1, 0.97, 0.94, and 0.92, respectively (Figure 7(a)). If γ is fixed, $|T_\lambda|$ also increases with the increase of parameter λ. It not only indicates that the joint with a smaller aperture generates more wave transmission across the joint but also that the rapid closure of the joint makes the joint stiffness increase faster. The overall growth trends of $|T_\lambda|$ in Figures 7(a) and 7(b) are similar. However, the curves of $|T_\lambda|$ at low frequency display an upward convex trend, while at high frequency, the S-shapes appear. $|T_\lambda|$ at low frequency is greater than that at high frequency when λ and γ are the same.

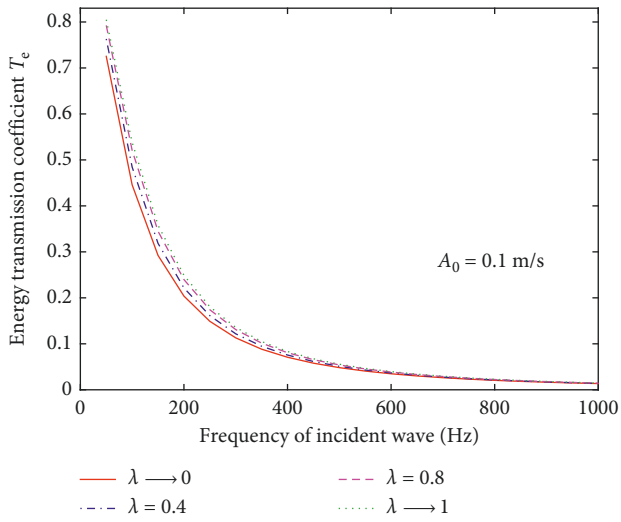

Figure 6: Effect of frequency on the energy transmission coefficient with different λ values.

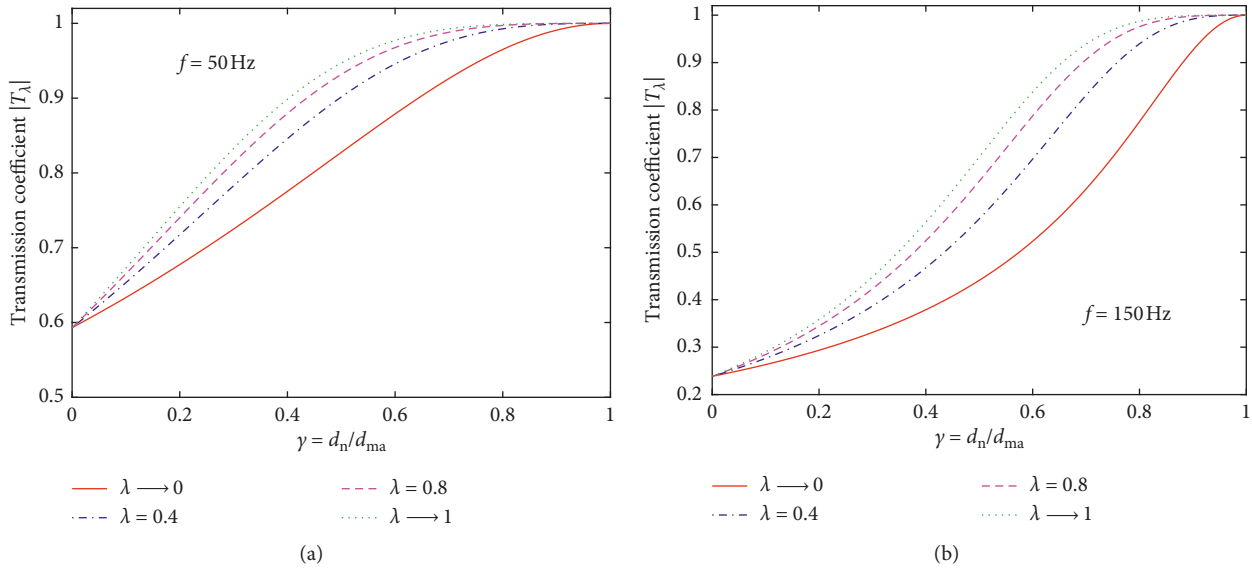

Figure 7: Transmission coefficient $|T_\lambda|$ as a function of γ for different λ values.

Similarly, the reflection coefficient $|R_\lambda|$ for four different values of λ gradually decreases until 0 with the increase of γ by using equation (24), as shown in Figure 8. For a given γ, $|R_\lambda|$ decreases with increasing λ. From the point of view of energy conservation and without considering energy loss, the energy of the transmitted wave passing through the joint increases, and the energy of the reflected wave decreases, and vice versa. The difference between Figures 8(a) and 8(b) is that $|R_\lambda|$ at low frequency is less than the high frequency when λ and γ are the same. As λ increases, the degree of the joint weathering is weaker and the amount of the joint closure is less, which leads to more transmitted waves and less reflected waves.

In general, the transmission coefficient of the nonlinear joint model (represented by $|T_{non}|$) is defined as the ratio of the transmitted wave's peak particle velocity to the incident wave's amplitude [10, 19, 36, 38]. However, the approximate analytical solution of the transmission coefficient $|T_\lambda|$ in the present study is based on the viewpoint of damage mechanics, and the equivalent stiffness is used to replace the stiffness constants in equation (20). The difference between the two methods is compared using the combination of parameters listed in Table 3. It can be observed that $|T_\lambda|$ and $|T_{non}|$ have a slight deviation, as shown in Figure 9. The deviation gradually decreases as the joint stiffness increases and maximum allowable joint closure decreases. This phenomenon indicates that the joint stiffness and the joint closure have a significant effect on the transmission coefficient calculated by the two methods. Therefore, if the joint stiffness is large and the amount of joint closure is little, it is a simple and convenient method to deduce the transmission coefficient $|T_\lambda|$ and the reflection coefficient $|R_\lambda|$, ignoring the lengthy mathematical derivation process.

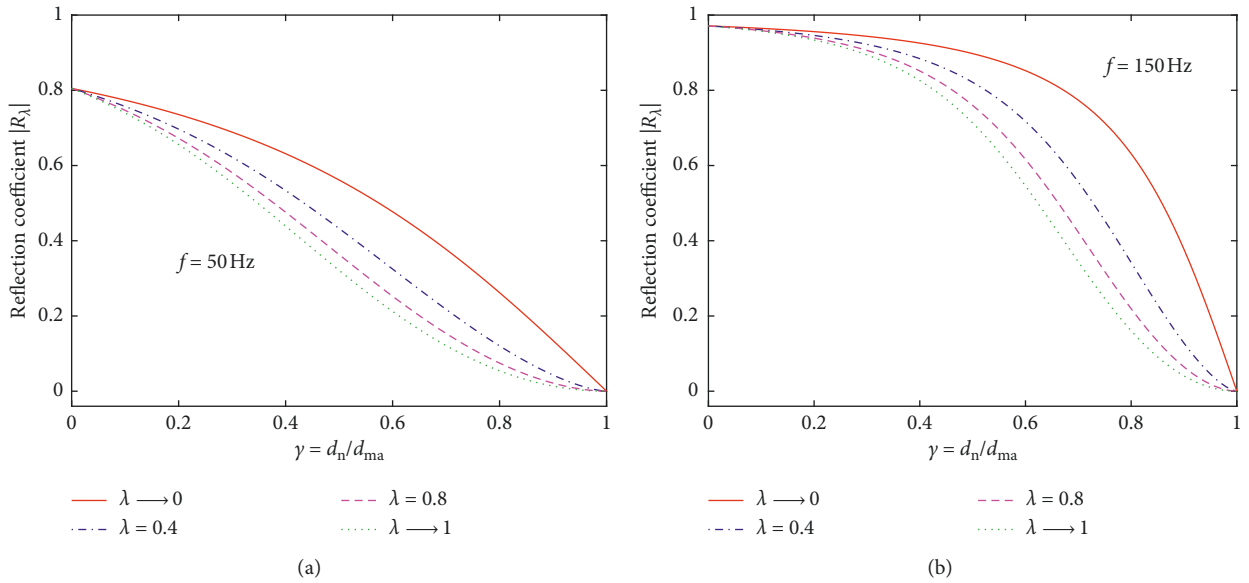

Figure 8: Reflection coefficient $|R_\lambda|$ as a function of γ for different λ values.

Table 3: Different values of k_{ni} and d_{ma} [19].

Parameter	k_{ni} (GPa/m)	d_{ma} (mm)
1	2.0	0.57
2	3.0	0.53
3	5.5	0.4

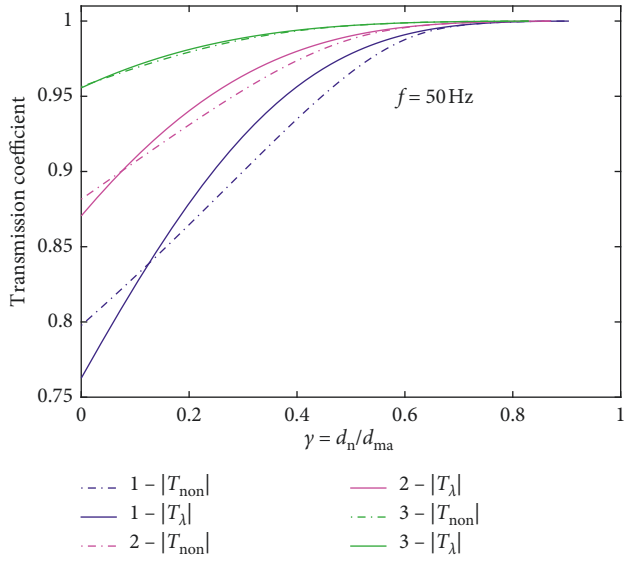

Figure 9: Transmission coefficient as a function of γ according to two methods.

4. Conclusions

The g-λ model (a normal deformation constitutive model of the joint) is adopted to analyze a P-wave propagating through a nonwelded single joint. The following main conclusions are drawn:

(1) The maximum amplitude of the transmitted wave increases gradually with the increase of parameter λ when using a half-sine wave as the incident wave. The waveform of the transmitted wave is like the waveform of the incident wave, but the phase has a delay. If $\lambda \longrightarrow 0$, the transmitted wave is closer to the conclusion of the classical exponential model, while $\lambda \longrightarrow 1$, it is in agreement with that of the BB model. It shows that the extension of the g-λ model from the static loading to the dynamic loading is feasible.

(2) The energy transmission increases with the increase of the incident wave's amplitude and decreases with the increase of the incident wave's frequency. It also increases with the increase of λ when the amplitude is fixed. The filtering effect of the joint is further confirmed. However, parameter λ has little effect on the energy transmission if the frequency is constant.

(3) The magnitude of the transmission and reflection coefficients depends on the joint stiffness and the extent of nonlinearity of rock joint deformation behavior. The transmission coefficient increases and the reflection coefficient decreases with the increase of λ. Besides, two methods calculating the transmission coefficient have less deviation when the joint stiffness increases and the maximum allowable closure of joint decreases.

Further studies are required to verify the accuracy of the g-λ model with different types of rock loading tests and nonlinear deformation behavior of joint as the P-wave obliquely propagates through a jointed rock mass.

Data Availability

The data used to support the findings of this study are available from the corresponding author upon request.

Conflicts of Interest

The authors declare that there are no conflicts of interest.

Acknowledgments

This work was supported by the National Key Research and Development Program of China (2016YFB1200401) and the Western Construction Project of the Ministry of Transport (2015318J29040).

References

[1] W. I. Fourney, R. D. Dick, X. J. Wang, and T. A. Weaver, "Effects of weak layers on particle velocity measurements," *Rock Mechanics and Rock Engineering*, vol. 30, no. 1, pp. 1–18, 1997.

[2] S. C. Fan, Y. Y. Jiao, and J. Zhao, "On modelling of incident boundary for wave propagation in jointed rock masses using discrete element method," *Computers and Geotechnics*, vol. 31, no. 1, pp. 57–66, 2004.

[3] Z. Wu and L. Fan, "The numerical manifold method for elastic wave propagation in rock with time-dependent absorbing boundary conditions," *Engineering Analysis with Boundary Elements*, vol. 46, pp. 41–50, 2014.

[4] X. Li, T. Zhou, D. Li, and Z. Wang, "Experimental and numerical investigations on feasibility and validity of prismatic rock specimen in SHPB," *Shock and Vibration*, vol. 2016, Article ID 7198980, 13 pages, 2016.

[5] X. B. Zhao, J. Zhao, and J. G. Cai, "P-wave transmission across fractures with nonlinear deformational behaviour," *International Journal for Numerical and Analytical Methods in Geomechanics*, vol. 30, no. 11, pp. 1097–1112, 2006.

[6] X. B. Zhao, J. B. Zhu, J. Zhao, and J. G. Cai, "Study of wave attenuation across parallel fractures using propagator matrix method," *International Journal for Numerical and Analytical Methods in Geomechanics*, vol. 36, no. 10, pp. 1264–1279, 2012.

[7] X. F. Deng, J. B. Zhu, S. G. Chen, and J. Zhao, "Some fundamental issues and verification of 3DEC in modeling wave propagation in jointed rock masses," *Rock Mechanics and Rock Engineering*, vol. 45, no. 5, pp. 943–951, 2012.

[8] W. Wu, J. B. Zhu, and J. Zhao, "A further study on seismic response of a set of parallel rock fractures filled with viscoelastic materials," *Geophysical Journal International*, vol. 192, no. 2, pp. 671–675, 2013.

[9] W. Wang, H. Hao, X. Li, Z. Yan, and F. Gong, "Effects of a single open joint on energy transmission coefficients of stress waves with different waveforms," *Rock Mechanics and Rock Engineering*, vol. 48, no. 5, pp. 2157–2166, 2015.

[10] J. C. Li, N. N. Li, H. B. Li, and J. Zhao, "An SHPB test study on wave propagation across rock masses with different contact area ratios of joint," *International Journal of Impact Engineering*, vol. 105, pp. 109–116, 2017.

[11] Z.-H. Zhang, J.-H. Deng, and J.-B. Zhu, "A rapid and nondestructive method to determine normal and shear stiffness of a single rock joint based on 1D wave-propagation theory," *Geophysics*, vol. 83, no. 1, pp. WA89–WA100, 2018.

[12] J. C. Li, L. F. Rong, H. B. Li, and S. N. Hong, "An SHPB test study on stress wave energy attenuation in jointed rock masses," *Rock Mechanics and Rock Engineering*, vol. 52, no. 2, pp. 403–420, 2019.

[13] L. F. Fan, Z. J. Wu, Z. Wan, and J. W. Gao, "Experimental investigation of thermal effects on dynamic behavior of granite," *Applied Thermal Engineering*, vol. 125, pp. 94–103, 2017.

[14] L. F. Fan, L. J. Wang, and Z. J. Wu, "Wave transmission across linearly jointed complex rock masses," *International Journal of Rock Mechanics and Mining Sciences*, vol. 112, pp. 193–200, 2018.

[15] R. E. Goodman, "The mechanical properties of joints," in *Proceedings of the Third Congress on ISRM, Volume 1A*, pp. 127–140, National Academy of Sciences, Denver, CO, USA, September 1974.

[16] R. E. Goodman, *Methods of Geological Engineering in Discontinuous Rock*, West, New York, NY, USA, 1976.

[17] S. C. Bandis, A. C. Lumsden, and N. R. Barton, "Fundamentals of rock joint deformation," *International Journal of Rock Mechanics and Mining Sciences and Geomechanics Abstracts*, vol. 20, no. 6, pp. 249–268, 1983.

[18] N. Barton, S. Bandis, and K. Bakhtar, "Strength, deformation and conductivity coupling of rock joints," *International Journal of Rock Mechanics and Mining Sciences and Geomechanics Abstracts*, vol. 22, no. 3, pp. 121–140, 1985.

[19] J. Zhao and J. G. Cai, "Transmission of elastic P-waves across single fractures with a nonlinear normal deformational behavior," *Rock Mechanics and Rock Engineering*, vol. 34, no. 1, pp. 3–22, 2001.

[20] J. G. Cai and J. Zhao, "Effects of multiple parallel fractures on apparent attenuation of stress waves in rock masses," *International Journal of Rock Mechanics and Mining Sciences*, vol. 37, no. 4, pp. 661–682, 2000.

[21] L. F. Fan and L. N. Y. Wong, "Stress wave transmission across a filled joint with different loading/unloading behavior," *International Journal of Rock Mechanics and Mining Sciences*, vol. 60, pp. 227–234, 2013.

[22] L. F. Fan and H. Y. Sun, "Seismic wave propagation through an in-situ stressed rock mass," *Journal of Applied Geophysics*, vol. 121, pp. 13–20, 2015.

[23] Z. Sun, C. Gerrard, and O. Stephansson, "Rock joint compliance tests for compression and shear loads," *International Journal of Rock Mechanics and Mining Sciences and Geomechanics Abstracts*, vol. 22, no. 4, pp. 197–213, 1985.

[24] K. Matsuki, E. Q. Wang, K. Sakaguchi, and K. Okumura, "Time-dependent closure of a fracture with rough surfaces under constant normal stress," *International Journal of Rock Mechanics and Mining Sciences*, vol. 38, no. 5, pp. 607–619, 2001.

[25] B. Malama and P. H. S. W. Kulatilake, "Models for normal fracture deformation under compressive loading," *International Journal of Rock Mechanics and Mining Sciences*, vol. 40, no. 6, pp. 893–901, 2003.

[26] J. Yu, X. B. Zhao, W. B. Zhao, X. Z. Li, and Y. F. Guan, "Improved nonlinear elastic constitutive model for normal deformation of rock fractures," *Chinese Journal of Geotechnical Engineering*, vol. 30, pp. 1316–1321, 2008, in Chinese.

[27] G. Rong, K. Huang, C. Zhou, X. Wang, and J. Peng, "A new constitutive law for the nonlinear normal deformation of rock joints under normal load," *Science China Technological Sciences*, vol. 55, no. 2, pp. 555–567, 2012.

[28] J. C. Li, W. Wu, H. B. Li, J. B. Zhu, and J. Zhao, "A thin-layer interface model for wave propagation through filled rock joints," *Journal of Applied Geophysics*, vol. 91, pp. 31–38, 2013.

[29] M. Schoenberg, "Elastic wave behavior across linear slip interfaces," *Journal of the Acoustical Society of America*, vol. 68, no. 5, pp. 1516–1521, 1980.

[30] L. J. Pyrak-Nolte, L. R. Myer, and N. G. W. Cook, "Transmission of seismic waves across single natural fractures,"

Journal of Geophysical Research, vol. 95, no. B6, pp. 8617–8638, 1990.

[31] Y. Li, Z. Zhu, B. Li, J. Deng, and H. Xie, "Study on the transmission and reflection of stress waves across joints," *International Journal of Rock Mechanics and Mining Sciences*, vol. 48, no. 3, pp. 364–371, 2011.

[32] J. C. Li, X. B. Zhao, H. B. Li, S. B. Chai, and Q. H. Zhao, "Analytical study for stress wave interaction with rock joints having unequally close-open behavior," *Rock Mechanics and Rock Engineering*, vol. 49, no. 8, pp. 3155–3164, 2016.

[33] Z. Fan, J. Zhang, and H. Xu, "Theoretical study of the dynamic response of a circular lined tunnel with an imperfect interface subjected to incident SV-waves," *Computers and Geotechnics*, vol. 110, pp. 308–318, 2019.

[34] X. B. Zhao, J. Zhao, J. G. Cai, and A. M. Hefny, "UDEC modelling on wave propagation across fractured rock masses," *Computers and Geotechnics*, vol. 35, no. 1, pp. 97–104, 2008.

[35] J. Lemaitre and J. L. Chaboche, *Mechanics of Solid Materials*, Cambridge University Press, Cambridge, UK, 1990.

[36] J. B. Zhu, A. Perino, G. F. Zhao et al., "Seismic response of a single and a set of filled joints of viscoelastic deformational behaviour," *Geophysical Journal International*, vol. 186, no. 3, pp. 1315–1330, 2011.

[37] J. B. Zhu and J. Zhao, "Obliquely incident wave propagation across rock joints with virtual wave source method," *Journal of Applied Geophysics*, vol. 88, pp. 23–30, 2013.

[38] Y. Zou, J. Li, L. Laloui, and J. Zhao, "Analytical time-domain solution of plane wave propagation across a viscoelastic rock joint," *Rock Mechanics and Rock Engineering*, vol. 50, no. 10, pp. 2731–2747, 2017.

[39] J. C. Li, G. W. Ma, and J. Zhao, "An equivalent viscoelastic model for rock mass with parallel joints," *Journal of Geophysical Research*, vol. 115, pp. 1–10, 2010.